Virologica Sinica 40 (2025) 388–400

Contents lists available at ScienceDirect

Virologica Sinica

journal homepage: www.keaipublishing.com/en/journals/virologica-sinica
www.virosin.org

Research article

Nucleophosmin 1 inhibits the replication of influenza A virus by competitively binding viral RNA with viral proteins

Yingying Yu [a], Qian Wang [a], Yanli Wei [a], Junwen Liu [a], Guangwen Wang [b], Zhengxiang Wang [a], Wentao Shen [a], Lu Han [a], Chengjun Li [b], Cao-Qi Lei [c], Shuai Xu [a,d,*], Qiyun Zhu [a,*]

[a] State Key Laboratory for Animal Disease Control and Prevention, College of Veterinary Medicine, Lanzhou University, Lanzhou Veterinary Research Institute, Chinese Academy of Agricultural Sciences, Lanzhou, 730000, China
[b] State Key Laboratory for Animal Disease Control and Prevention, Harbin Veterinary Research Institute, Chinese Academy of Agricultural Sciences, Harbin, 150069, China
[c] State Key Laboratory of Virology, College of Life Sciences, Wuhan University, Wuhan, 430072, China
[d] Gansu Province Research Center for Basic Disciplines of Pathogen Biology, Lanzhou, 730046, China

ARTICLE INFO

Keywords:
Nucleophosmin-1 (NPM1)
Influenza A virus (IAV)
RNA binding
Viral RNA
Viral polymerase

ABSTRACT

Influenza A viruses (IAVs) are single-stranded negative-sense RNA viruses that continually challenge animal and human health. In IAV-infected cells, host RNA-binding proteins play key roles in the life cycle of IAV by directly binding to viral RNA. Here, we examined the role of the host RNA-binding protein nucleophosmin-1 (NPM1) in IAV replication. We found that, as a nucleolar phosphoprotein, NPM1 directly binds to viral RNA (vRNA) and inhibits the replication of various subtypes of IAV. NPM1 binding to vRNA competitively reduces the assembly of the viral ribonucleoprotein complex and the viral polymerase activity, thereby reducing the generation of progeny viral RNA and virions. The RNA-binding activity of NPM1, with the key residues T199, T219, T234, and T237, is essential for its anti-influenza function. Taken together, our findings demonstrate that NPM1 acts as an RNA-binding protein and interacts with IAV vRNA to suppress viral replication.

INTRODUCTION

Influenza A viruses (IAVs) are important zoonotic pathogens that pose a continuous challenge to avian and mammalian species, including humans (Wasik et al., 2021; Krammer and Schultz-Cherry, 2023). Since 1918, IAVs have caused at least four influenza pandemics and considerable loss of human life (Taubenberger and Kash, 2010). In addition, an increasing number of avian influenza viruses, such as H5N1, H7N9, H9N2, and recently H3N8, have acquired the ability to cross the species barrier to infect humans (Gao et al., 2013; Zhang et al., 2013; Yang et al., 2023; Sun et al., 2023).

IAVs are segmented, single-stranded, negative-sense RNA viruses that are members of the *Orthomyxoviridae* family (Eisfeld et al., 2015; Lakdawala et al., 2014). The heterotrimeric influenza polymerase, consisting of basic polymerase 2 (PB2), basic polymerase 1 (PB1), and acidic polymerase (PA), binds to the eight viral RNA (vRNA) segments, which are packaged by the viral nucleoprotein (NP) into ribonucleoprotein complexes (vRNPs). For IAV, replication primarily occurs in the nucleus. Upon virus entry into the infected cell, vRNPs are transported to the nucleus, where they generate viral mRNA for viral protein synthesis. The same vRNPs perform the replication of vRNA into complementary RNA (cRNA), for the production of progeny vRNA (Fan et al., 2019).

During IAV replication, various RNA-binding proteins (RBPs) have been identified as key factors regulating viral replication through their direct binding to viral RNA. In cells infected with IAV, the viral RNA is recognized by several RBPs, including retinoic acid-inducible gene I (RIG-I) and Z-DNA binding protein 1 (ZBP1), which are known as pattern recognition receptors (PRRs) and initiate downstream antiviral signaling (Kato et al., 2006; Zhang et al., 2020). Another RBP, human polyadenylate binding protein 1 (PABP1), binds to the 5′UTR of the viral mRNAs and promotes translation initiation of IAVs (de Rozieres et al., 2022). In addition, host adenosine deaminase ADAR-1 may hyper-deaminate adenosine residues in IAV genomes, leading to both A→G and U→C substitutions, and restricting the replication of IAV (Suspene et al., 2011). Zhu et al. reported that the N^6-methyladenosine reader protein YTHDC1 directly binds to the 3′ splicing site of IAV

* Corresponding authors.
E-mail addresses: zhuqiyun@caas.cn (Q. Zhu), xushuai@caas.cn (S. Xu).

https://doi.org/10.1016/j.virs.2025.04.007
Received 16 December 2024; Accepted 27 April 2025
Available online 6 June 2025
1995-820X/© 2025 The Authors. Publishing services by Elsevier B.V. on behalf of KeAi Communications Co. Ltd. This is an open access article under the CC BY-NC-ND license (http://creativecommons.org/licenses/by-nc-nd/4.0/).

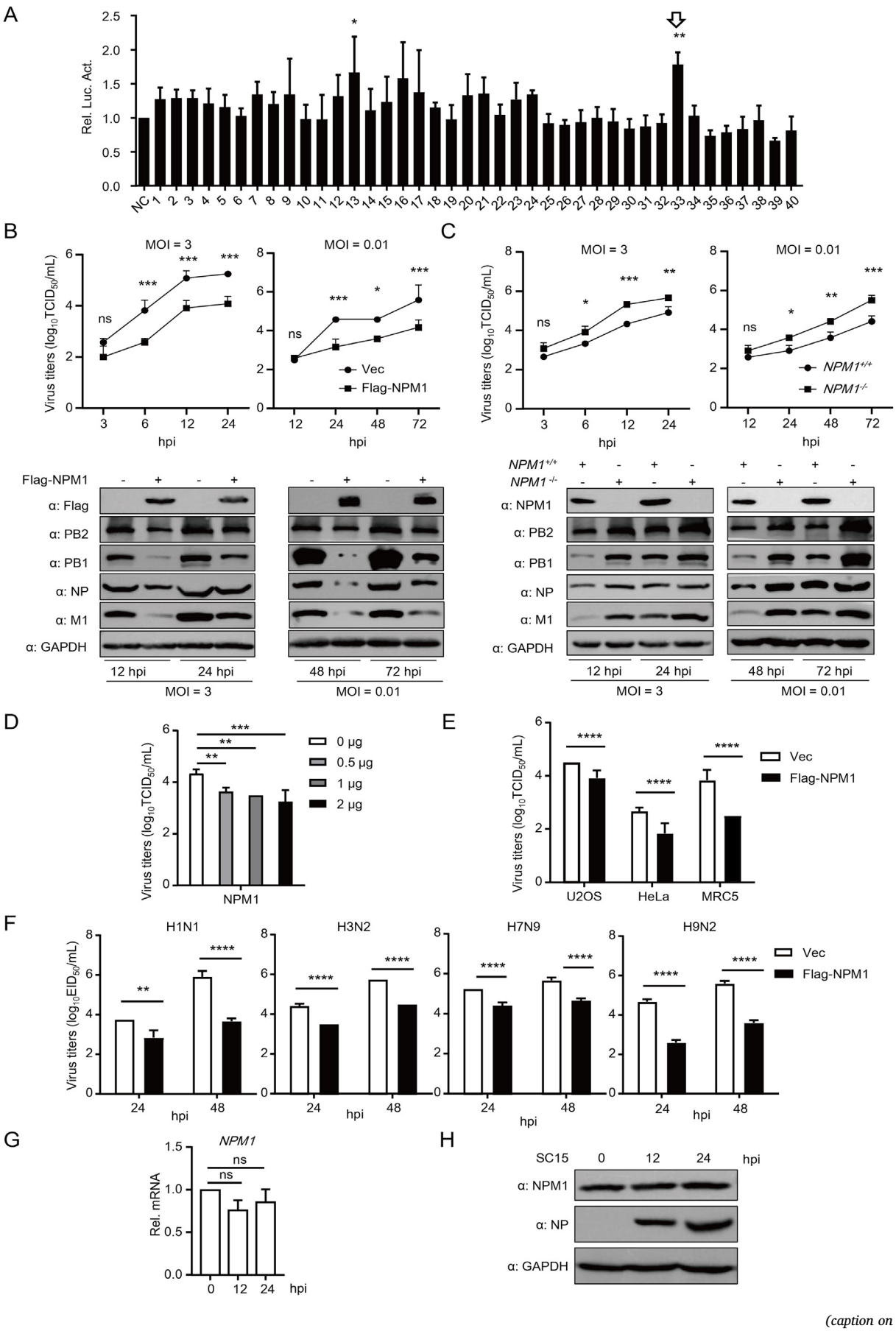

(caption on next page)

Fig. 1. NPM1 significantly inhibits the replication of influenza A virus. **A** A549 cells were transfected with the indicated siRNAs and 24 h later infected with the reporter virus. Supernatants were collected from the cells 24 h post-infection and used for luciferase assays. **B** A549 cells were transfected with either the NPM1 expression plasmid or an empty vector (Vec). Twenty-four hours later, the cells were infected with H5N6 influenza virus (SC15 strain) at a multiplicity of infection (MOI) of 3.0 or 0.01. At the indicated times post-infection, the supernatant containing viral particles was assessed in the $TCID_{50}$ assay. Expression levels of Flag-NPM1 and viral proteins were quantified at indicated times. **C** *NPM1*$^{+/+}$ or *NPM1*$^{-/-}$ A549 cells were infected with SC15 strain at an MOI of 3.0 or 0.01. At the indicated times post-infection, the supernatant containing viral particles was assessed in the $TCID_{50}$ assay. Expression levels of Flag-NPM1 and viral proteins were quantified at indicated times. **D** A549 cells were transfected with increasing amounts of NPM1 expression plasmids. Twenty-four hours post-infection, the expression level of Flag-NPM1 was quantified, and the supernatant containing viral particles was assessed in the $TCID_{50}$ assay. **E** U2OS, HeLa, and MRC5 cells were transfected with either the NPM1 expression plasmid or Vec. Twenty-four hours later, the cells were infected with SC15 strain at an MOI of 0.01. Twenty-four hours post-infection, the supernatant containing viral particles was assessed in the $TCID_{50}$ assay. **F** A549 cells were transfected with either the NPM1 expression plasmid or Vec. Twenty-four hours later, the cells were infected with H1N1, H3N2, H7N9, or H9N2 viruses at an MOI of 0.01. At 24 and 48 h post-infection, the supernatant containing viral particles was assessed in the EID_{50} assay. **G** A549 cells were infected with SC15 strain (MOI = 1), and the NPM1 mRNA was quantified at different times post-infection by use of qPCR analysis. **H** A549 cells were infected with SC15 virus (MOI = 1), and the expression level of NPM1 protein was quantified at indicated times post-infection. The data shown represent three independent experiments; bars represent the mean ± SD of the three independent experiments (n = 3). $^{*}P < 0.05$, $^{**}P < 0.01$, $^{***}P < 0.001$, $^{****}P < 0.0001$; 'ns' indicates no significant difference.

non-structural (NS) segment, and inhibits the splicing of NS mRNA in IAV-infected cells (Zhu et al., 2023). However, the functional interplay between host RBPs and IAV RNA remains largely unknown.

Nucleolar phosphoprotein nucleophosmin-1 (NPM1, also known as B23) is highly conserved across various vertebrates such as humans, chickens, and fish, and possesses RNA-binding activity through its central region and C-terminal domain (Hisaoka et al., 2014). NPM1 plays a part in multiple cellular functions, such as genomic stability, ribosome biogenesis, chromatin remodeling, centrosome duplication, and nucleus-cytoplasm transport (Karimi Dermani et al., 2021). Furthermore, NPM1 has been reported to have functional roles in the replication of various viruses by interacting with viral proteins. HIV-1 infection induces acetylation of NPM1, which then interacts with the HIV-Tat protein, and is critical for the nuclear localization of Tat as well as Tat-mediated transcription (Stauber and Pavlakis, 1998; Gadad et al., 2011). In addition, the N protein of SARS-CoV-2 has been shown to interact with NPM1 and small nucleolar RNAs (snoRNAs), boosting ribosome translation efficiency, particularly for viral mRNAs, thereby promoting the replication of the virus (Wang et al., 2022). However, few studies have focused on the specific role of NPM1 as an RBP in the life cycle of viruses, especially IAVs.

In the present study, we revealed that NPM1 is a negative regulator of IAV replication, significantly inhibiting the replication of multiple subtypes of IAVs. Mechanistically, NPM1 does not directly interact with the vRNP proteins of IAV; rather, it binds directly to the viral RNA through its RNA-binding activity, inhibiting the binding of vRNP proteins to the viral RNA, thereby impeding viral replication.

RESULTS

Identification of NPM1 as a candidate inhibitor of IAV replication

To identify potential host RBPs that participate in the life cycle of IAV, we synthesized an small interfering RNA (siRNA) library containing a series of host RBP genes. Based on the strategy described by Nogales et al., a bioluminescent reporter virus (PR8-NLuc) was generated using reverse genetics as a "biomarker" of virus replication (Chiem et al., 2019). Using this reporter virus and siRNA library, we identified several genes that exhibited regulatory functions in the replication of IAV (Fig. 1A). Among them, the luciferase activity of the 33rd siRNA (targeting the *NPM1* gene)-treated cells was significantly higher than that in the negative control (NC)-treated cells (Fig. 1A).

The effect of NPM1 on IAV replication was further evaluated with wild-type viruses. Overexpression of NPM1 significantly inhibited the replication of H5N6 influenza virus (SC15 strain), whereas NPM1 deficiency significantly facilitated viral replication (Fig. 1B and C). In addition, NPM1 inhibited virus growth in a dose-dependent manner, and in various cell lines (Fig. 1D and E). Furthermore, NPM1 inhibited the replication of H1N1, H3N2, H7N9, and H9N2 viruses in A549 cells (Fig. 1F). In addition, IAV infection showed slight effect to the expression of NPM1 (Fig. 1G and H).

We next explored whether NPM1 interacts with viral proteins. Co-immunoprecipitation (co-IP) results indicated that endogenous NPM1 does not interacts with NP, as well as other viral proteins (Fig. 2A). Considering the nuclear location of NPM1, we investigated whether NPM1 affects the viral polymerase activity of IAV by using a minigenome assay. Overexpression of NPM1 deceased polymerase activity in a dose-dependent manner, whereas knockdown of NPM1 enhanced viral polymerase activity (Fig. 2B and C). The *in vitro* polymerase assay, which was conducted as previously described (Wang et al., 2025), indicated that NPM1 inhibits the polymerase activity of influenza virus (Fig. 2D and E). Similarly, NPM1 overexpression significantly decreased the expression of vRNA, as well as cRNA and mRNA, and knockdown of NPM1 facilitated the expression of vRNA, cRNA, and mRNA of IAV (Fig. 2F and G). Using cycloheximide (CHX) to inhibit viral protein synthesis and genome replication, NPM1 reduced the expression level of vRNA, as well as the synthesis of mRNA from vRNA (Fig. 2H). These data suggest that NPM1 may inhibit the replication of IAV by inhibiting viral polymerase activity during the replication and transcription of the viral RNA.

NPM1 directly binds to viral RNA of IAV

Using formaldehyde cross-linked RIP (CLIP) and qRT-PCR methods, we confirmed that all eight segments of viral RNA in IAV-infected cells were pulled down by NPM1 (Fig. 3A), and NPM1 interacted with viral RNA from different subtypes of IAVs (Fig. 3B). Using an RNA antisense purification (RAP) assay with biotin-labeled NP vRNA-specific probes, we detected the interaction between NP vRNA and NPM1 protein (Fig. 3C). Additionally, NPM1 directly interacted with viral RNA from purified virions (Fig. 3D). Microscopic analysis showed that GFP-NPM1 was mainly distributed in the nucleolus, and was observed a high degree of colocalization of GFP-NPM1 with vRNA (Fig. 3E). Therefore, these results demonstrate that the nucleolar NPM1 directly interacts with the viral RNA of IAV.

NPM1 inhibits the interaction between the vRNP proteins and the viral RNA of IAV

As shown in Fig. 3B, overexpressed NPM1 inhibits the interaction between NP vRNA and NP protein. Considering the fact that NPM1 inhibits viral polymerase activity and directly interacts with viral RNA, we next tested the effect of the NPM1-vRNA interaction on the vRNP complex. Our data from CLIP experiment revealed that NPM1 impairs the interaction between vRNA and vRNP proteins, namely PB2, PB1, PA, and NP (Fig. 4A). Knockdown of NPM1 enhanced the binding between vRNA and vRNP proteins (Fig. 4B). In the RAP assay, fewer vRNP proteins were pulled-down by the NP vRNA probes in NPM1-overexpressed cells (Fig. 4C), whereas more vRNP proteins were pulled-down in NPM1 knockdown cells (Fig. 4D). In addition, the vRNP proteins reduced the amount of NPM1 pulled-down by the NP

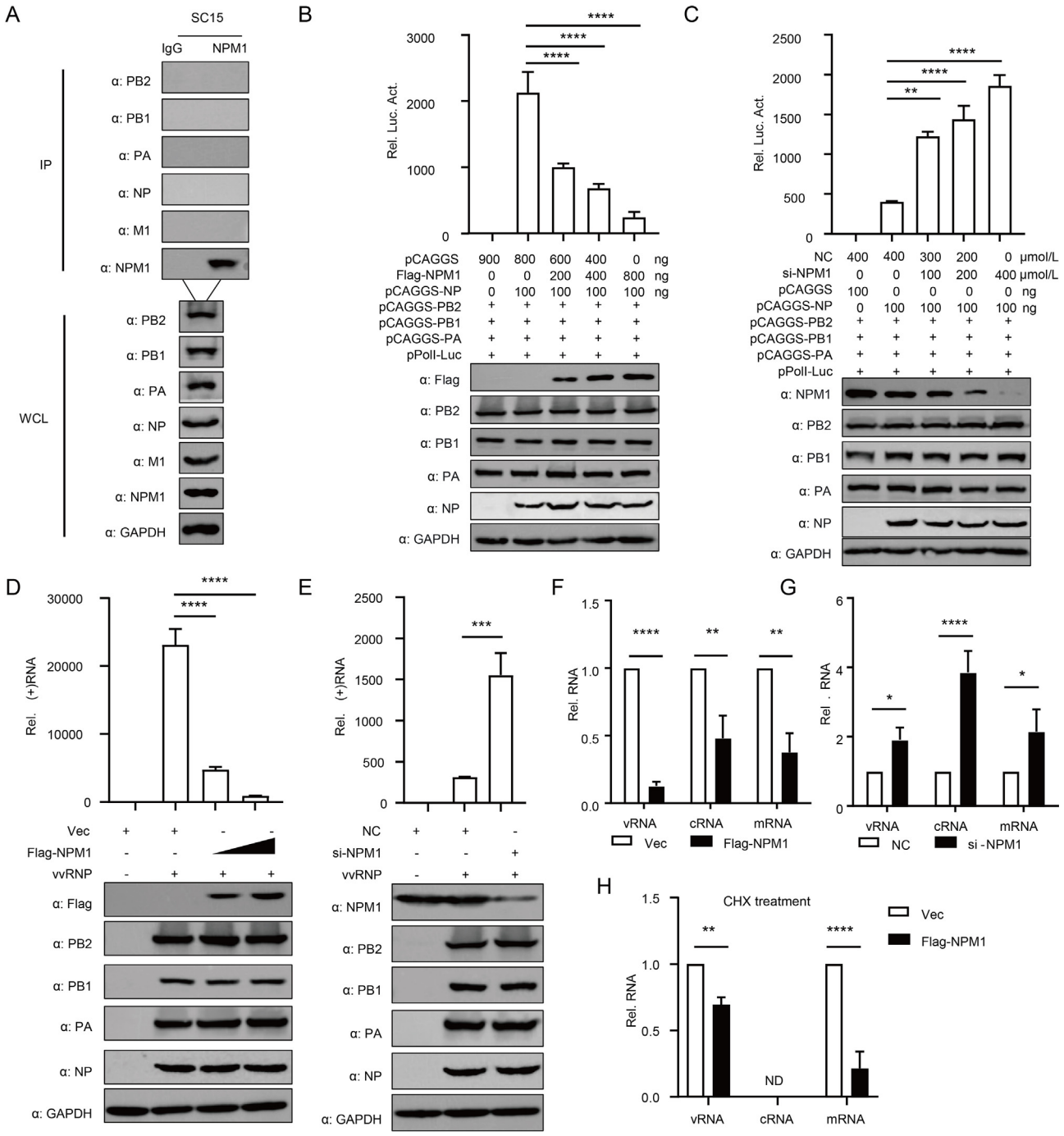

Fig. 2. NPM1 inhibits the viral polymerase activity. **A** HEK293T cells were infected with SC15 strain and the cell lysate was subjected to co-IP with IgG or anti-NPM1 antibody. **B** HEK293T cells were transfected with PB2, PB1, PA, NP, and pPolI-Luc and TK reporter constructs, together with increasing amounts of NPM1 expression plasmids. Luciferase activities were measured. Data shown represent the ratio of the luciferase activity in each group normalized to that in the control group without NP (Ctrl). **C** HEK293T cells were transfected with PB2, PB1, PA, NP, and pPolI-Luc and TK reporter constructs, together with increasing amounts of NPM1 siRNA. Data shown represent the ratio of the luciferase activity in each group normalized to that in the control group without NP (Ctrl). **D** HEK293T cells were transfected with Flag-NPM1. The cell lysates were incubated with purified virion vRNP (vvRNP). In the negative control group, vvRNP were omitted. The lower immunoblots showed the expression level of viral proteins and Flag-NPM1. **E** HEK293T cells were transfected with NPM1 siRNA or NC. The cell lysates were incubated with purified virion vRNP (vvRNP). In the negative control group, vvRNP were omitted. The lower immunoblots showed the expression level of viral proteins and NPM1. **F** A549 cells were transfected with the NPM1 expression plasmid or Vec. Twenty-four hours later, the cells were infected with SC15 strain (MOI = 1) for 24 h, and total RNA was extracted for qRT-PCR to detect the expression of NP vRNA, cRNA, or mRNA. **G** A549 cells were transfected with the NPM1 siRNA or scrambled siRNA (NC). Twenty-four hours later, the cells were infected with SC15 strain (MOI = 1) for 24 h, and total RNA was extracted for qRT-PCR to detect the expression of NP vRNA, cRNA, or mRNA. **H** A549 cells were transfected with the NPM1 expression plasmid or Vec. Twenty-four hours later, the cells were infected with SC15 strain (MOI = 1) and treated with CHX (100 μg/mL) for 3 h, and total RNA was extracted for qRT-PCR to detect the expression of NP vRNA, cRNA, or mRNA. The data shown represent three independent experiments; bars represent the mean ± SD of the three independent experiments (n = 3). $^{*}P < 0.05$, $^{**}P < 0.01$, $^{***}P < 0.001$, $^{****}P < 0.0001$; 'ns' indicates no significant difference.

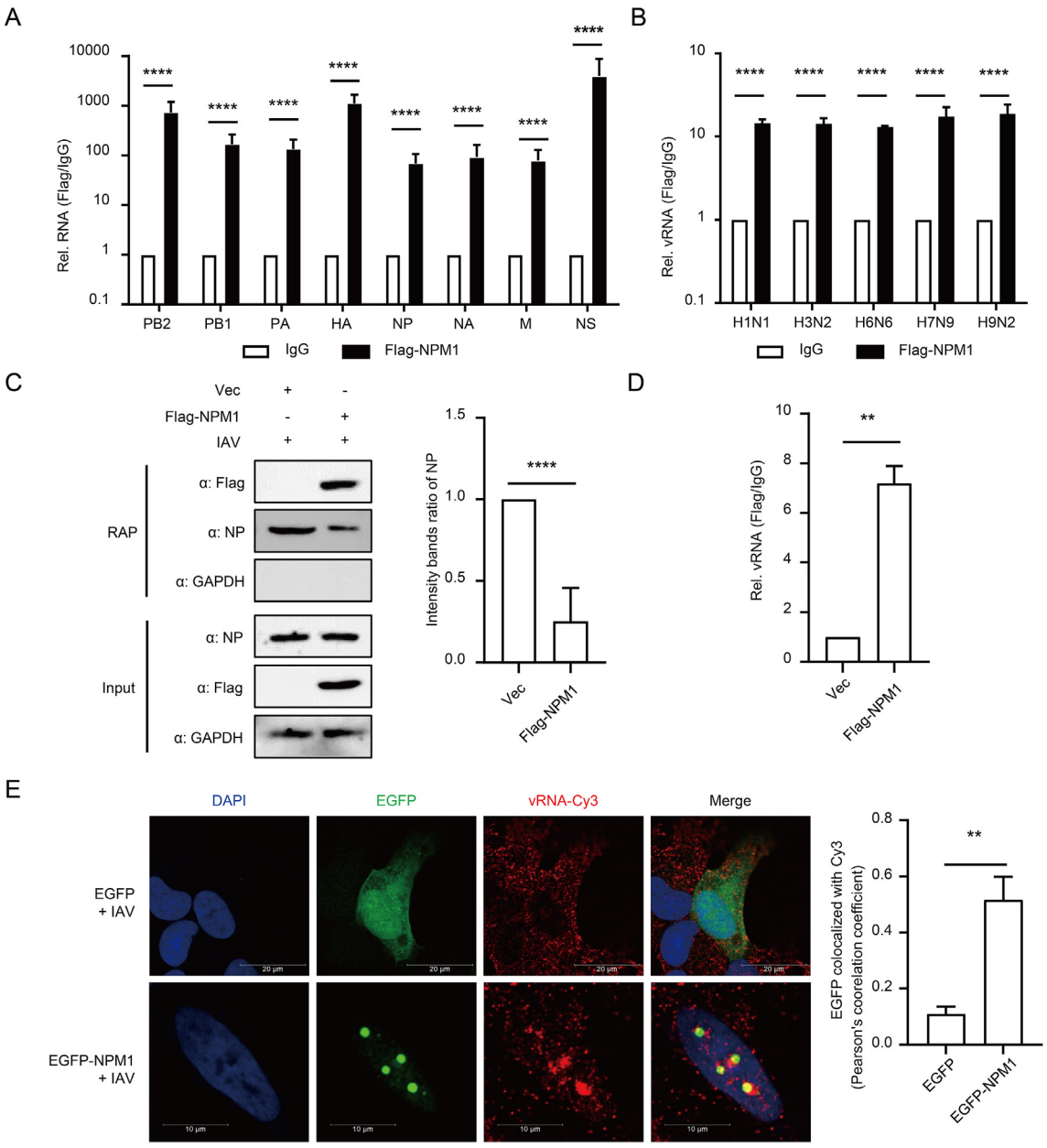

Fig. 3. NPM1 directly binds to the viral RNAs of IAV. **A** A549 cells were transfected with Flag-NPM1. Twenty-four hours later, the cells were infected with SC15 strain at an MOI of 1. Twenty-four hours post-infections, cells were formaldehyde-crosslinked, and cell lysates were subjected to IP with an anti-Flag antibody or IgG and quantified by qRT-PCR. **B** A549 cells were transfected with Flag-NPM1. Twenty-four hours later, the cells were infected with H1N1, H3N2, H7N9, or H9N2 viruses at an MOI of 1. Twenty-four hours post-infections, cells were formaldehyde-crosslinked, and cell lysates were subjected to IP with an anti-Flag antibody or IgG and quantified by qRT-PCR. **C** A549 cells were infected with SC15 strain (MOI = 0.1 for Vec, and MOI = 1 for Flag-NPM1) for 24 h. Next, the cells were formaldehyde-crosslinked, and the cell lysates were subjected to RNA antisense purification (RAP) assays using biotinylated antisense probes specific to IAV NP-vRNA. RNA-binding proteins were analyzed by Western blotting. The intensities of the NP bands in RAP were determined using ImageJ. **D** HEK293T cells were transfected with Flag-NPM1. The cell lysates were incubated with viral RNA from purified virion, and then were subjected to IP with an anti-Flag antibody or IgG and quantified by qRT-PCR. **E** U2OS cells were transfected with the EGFP-NPM1 expression plasmid. Twenty-four hours later, the cells were infected with SC15 strain for 12 h before fixing. The cells were stained with NP-vRNA-specific FISH probes before confocal microscopy. Scale bar: 20 μm. The right panel shows the quantification of Pearson's colocalization coefficient between EGFP and Cy3. The data shown represent three independent experiments; bars represent the mean ± SD of the three independent experiments (n = 3). $*P < 0.05$, $**P < 0.01$, $***P < 0.001$, $****P < 0.0001$; 'ns' indicates no significant difference.

vRNA probes (Fig. 4E). The *in vitro* CLIP assay indicated that NPM1 inhibits the interaction of viral RNA with RNP proteins (Fig. 4F). PB2, PB1, PA, and NP impeded the binding of NPM1 to vRNA (Fig. 4G). These results indicate that the NPM1-vRNA interaction inhibits the binding of vRNP proteins to the viral RNA.

Residues T199, T219, T234, and T237 of NPM1 are essential for NPM1-mediated inhibition of IAV replication

We next determined the structural basic of the NPM1-mediated inhibition of IAV replication. NPM1 has a modular structure comprising

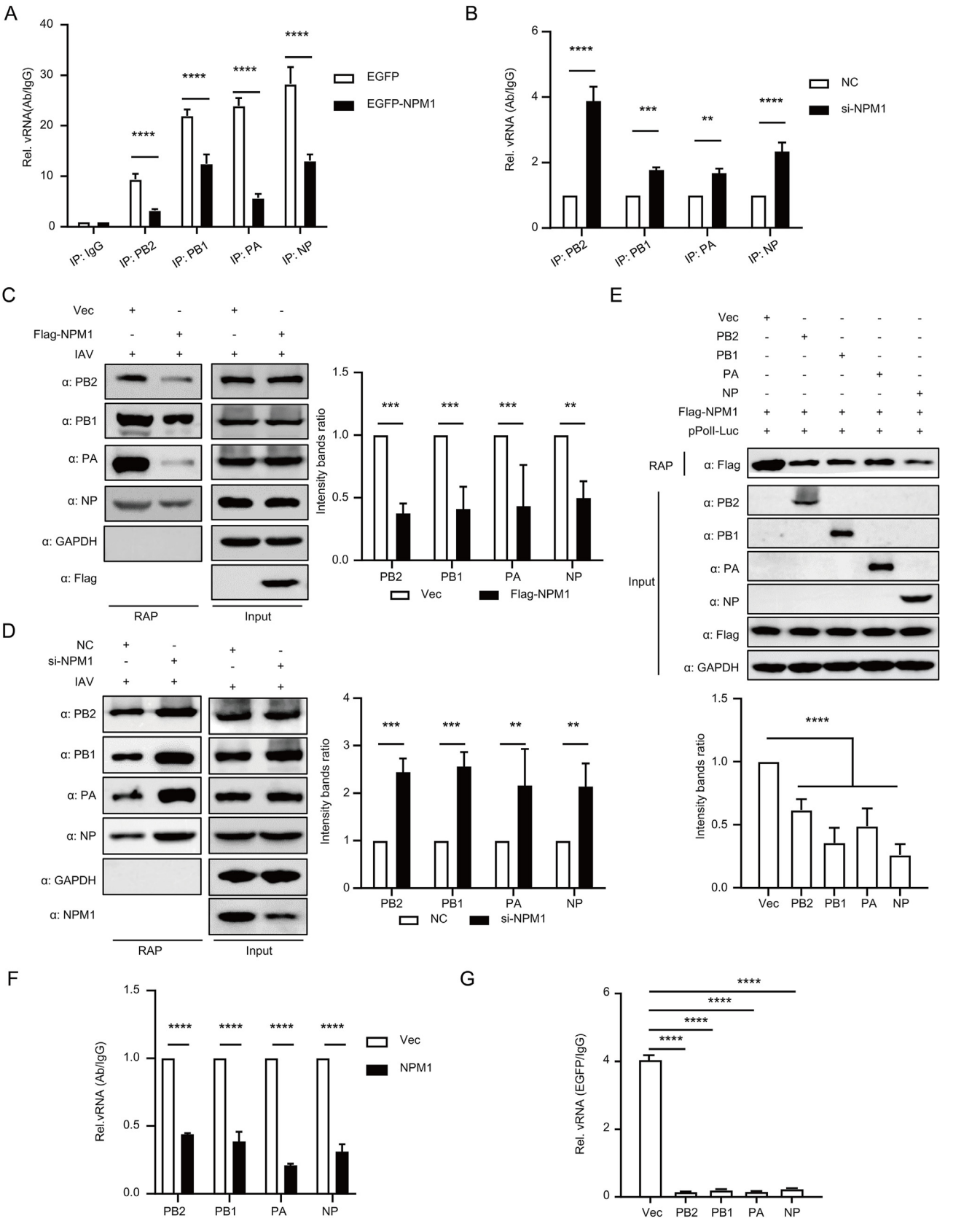

(caption on next page)

Fig. 4. NPM1 impairs the interaction of vRNP proteins with the viral RNA of influenza virus. **A** HEK293T cells were transfected with Flag-NPM1, PB2, PB1, PA, NP, and pPolI-Luc constructs, together with EGFP or EGFP-NPM1. Twenty-four hours later, the cells were subjected to a CLIP assay with PB2-, PB1-, PA-, and NP-specific antibodies, or IgG. **B** HEK293T cells were transfected with either NPM1 siRNA or NC, together with PB2, PB1, PA, NP, and pPolI-Luc constructs. Twenty-four hours later, the cells were subjected to the CLIP assay with PB2-, PB1-, PA-, and NP-specific antibodies or IgG. **C** HEK293T cells were transfected with the NPM1 expression plasmid or Vec. Twenty-four hours later, the cells were infected with SC15 strain (MOI = 0.1 for Vec, and MOI = 1 for Flag-NPM1) for 24 h. Twenty-four hours later, the cells were cross-linked with formaldehyde, and the cell lysates were subjected to RAP assays using biotinylated antisense probes targeting IAV NP-vRNA. RNA-binding proteins were analyzed by Western blotting. The intensities of the indicated bands in RAP were determined using ImageJ. **D** HEK293T cells were transfected with the NPM1 siRNA or scrambled siRNA (NC). Twenty-four hours later, the cells were infected with SC15 strain (MOI = 1 for NC, and MOI = 0.1 for si-NPM1) for 24 h. Then, cells were cross-linked with formaldehyde and subjected to RAP assays using biotinylated probes targeting NP-vRNA. RNA-binding proteins were analyzed by Western blotting. The intensities of the indicated bands in RAP were determined using ImageJ. **E** HEK293T cells were transfected with pPolI-Luc constructs and Flag-NPM1, together with Vec, PB2, PB1, PA, or NP. Twenty-four hours later, cells were crosslinked and subjected to RAP assays using biotinylated probes targeting NP-vRNA. RNA-binding proteins were analyzed by Western blotting. The intensities of the Flag-NPM bands in RAP were determined using ImageJ. **F** HEK293T cells were transfected with Flag-NPM1. The cell lysates were incubated with purified virion containing viral RNA and vRNP proteins, then were subjected to IP with PB2-, PB1-, PA-, and NP-specific antibodies or IgG, and quantified by qRT-PCR. **G** HEK293T cells were transfected with pPolI-Luc constructs and EGFP or EGFP-NPM1, together with Vec, PB2, PB1, PA or NP. Twenty-four hours later, the cells were subjected to a CLIP assay with EGFP-specific antibodies or IgG. The data shown represent three independent experiments; bars represent the mean ± SD of the three independent experiments (n = 3). $^{*}P < 0.05$, $^{**}P < 0.01$, $^{***}P < 0.001$, $^{****}P < 0.0001$; 'ns' indicates no significant difference.

folded N-terminal and C-terminal domains (NTD and CTD) linked by an intrinsically disordered region (IDR) (Saluri et al., 2023). Domain mapping failed to identify the specific domain that contributes to the suppression of IAV replication (data not shown).

Previous studies have revealed that the four threonine residues (T199, T219, T234, and T237) of NPM1 are important for its RNA-binding activity (Hisaoka et al., 2014; Okuwaki et al., 2002). We therefore generated a mutant with four threonine residues (T199A/T219A/-T234A/T237A, T4A) in the NPM1 protein (Fig. 5A). Consistent with previous results, the T4A mutant bound less vRNA in plasmid-transfected or virus-infected cells, compared with wild-type NPM1 (Fig. 5B and C). Moreover, less NPM1-T4A was pulled-down by NP vRNA probes (Fig. 5D). Confocal microscopy confirmed that NPM1-T4A was no longer mainly located in the nucleoli, but was dispersed in the nucleus (Fig. 5E). NPM1 reduced the interaction between NP and vRNA, which was reversed by the T4A mutant, in cells transfected with vRNP plasmids (Fig. 5F) or infected with virus (Fig. 5G).

Lastly, we determined the significance of NPM1-T4A to virus replication. The T4A mutant significantly restored the attenuation of virus growth caused by NPM1, in wild-type (Fig. 6A) or NPM1-deficient cells (Fig. 6B). In addition, T4A mutation restored the NPM1 caused attenuation of polymerase activity (Fig. 6C) and the reduced expression of vRNA, cRNA, and mRNA in virus-infected cells (Fig. 6D).

Our results collectively suggest that the T199, T219, T234, and T237 of NPM1 are essential for NPM1-mediated inhibition of IAV replication.

DISCUSSION

The nucleolus is a dynamic cellular structure and the largest membrane-less subcellular structure within the nucleus. It is involved in various biological processes, including ribosome biogenesis, transcription, cell cycle control, genomic stability, cellular aging, and viral infection (Pederson, 2011). However, little is known about the role of the nucleolus in the replication of influenza virus. Studies have revealed that the NS1 and NP proteins of IAV could accumulate in the nucleolus, due to nucleolar localization signals (Nguyen et al., 2023; Melen et al., 2012). Nucleolin is a nucleolar phosphoprotein that is abundantly present in the central region of the nucleolus. Several studies have revealed that nucleolin promotes virus replication by interacting with various viral proteins, such as NP and NS1 (Terrier et al., 2016; Yan et al., 2017). NPM1 is the primary component of the outermost nucleolar phase and of the granular component; as such, it is frequently utilized as a marker for the nucleolar granular component. In the present study, we found that NPM1 interacts with viral RNA of influenza A virus. The NPM1-vRNA interaction competitively inhibits the binding of viral proteins to vRNA, leading to reduced assembly of the vRNP complex and suppression of IAV replication. Further research is needed to explore the role of the nucleolus, especially nucleolus-based host factors, in the replication of IAV.

NPM1 is one of the most abundant nucleolar proteins, primarily localized in the nucleolus, and is known to shuttle between the nucleus and the cytoplasm (Borer et al., 1989). Importantly, NPM1 plays multiple roles in various stages of viral replication. Pradeep et al. have reported that NPM1 plays antiviral roles in Chikungunya virus (CHIKV) infection, which involve the translocation of NPM1 from the nucleus to the cytoplasm and binding with functional domains of CHIKV nonstructural protein 3 (Pradeep et al., 2023). NPM1 has been shown to be important for the nucleolar localization of the circovirus capsid protein through translocation from the nucleolus to the nucleoplasm and cytoplasm and direct interaction (Zhou et al., 2020, 2021). In cells infected with SARS-CoV-2, the NPM1-snoRNA translation machinery are potentiated by the SARS-CoV-2 N protein to promote ribosome translation efficiency, especially for viral mRNAs, by enhancing snoRNA-mediated 2′-*O*-methylation on rRNAs (Wang et al., 2022). In the present study, NPM1, as a nucleolar-localized matrix protein, inhibited vRNP complex assembly and viral polymerase activity through its RNA-binding activity, exerting an antiviral function.

NPM1 has a modular structure comprising a NTD and CTD linked by an IDR region (Saluri et al., 2023). The NTD of NPM1 adopts a β-sheet sandwich fold and enhances self-oligomerization to assemble into pentamers (Sakashita et al., 2018). Within nucleoli, NPM1 undergoes liquid–liquid phase separation (LLPS) through different mechanisms, one of which relies on the binding of the CTD and IDR region of NPM1 to RNA (Saluri et al., 2023). It is reasonable to hypothesize that NPM1 directly interacts with viral RNA in the nucleoli of IAV-infected cells. Our data showed that NPM1 binds vRNAs to inhibit the assembly of vRNP complex and the viral polymerase activity, and that the RNA-binding activity of NPM1 is essential for it to inhibit the replication of IAV. Although we failed to identify the key domain of NPM1 responsible for restricting the replication of IAV through domain mapping, it was found that mutation of the critical residue for the oligomerization of NPM1 blocked the inhibition of the replication of IAV (Prinos et al., 2011) (data not shown), which suggests that the functional integrity of NPM1 is a prerequisite for its anti-influenza activity.

In the present study, NPM1 was confirmed as a RBP to interact with viral RNA. Previous studies have claimed that NPM1 regulates IAV replication by interacting with NP protein, but these studies did not considered the RNA-binding activity of NPM1 (Mayer et al., 2007; Bortz et al., 2011). In addition, we found that overexpressed NPM1 from transfected plasmids tended not to localize in the nucleolus. Yet, the nucleolar localization of NPM1 is critical for its biological functions (Chiarella et al., 2013). All exogenous NPM1 proteins in this study showed clear nucleolar localization, similar to the endogenous NPM1 (Figs. 3E and 5E); however, the T4A mutant of NPM1 was not confined to the nucleolus, which may be one reason why NPM1-T4A did not reduce the replication of IAV. In future studies, special attention should be paid to the nucleolar localization of exogenously expressed NPM1.

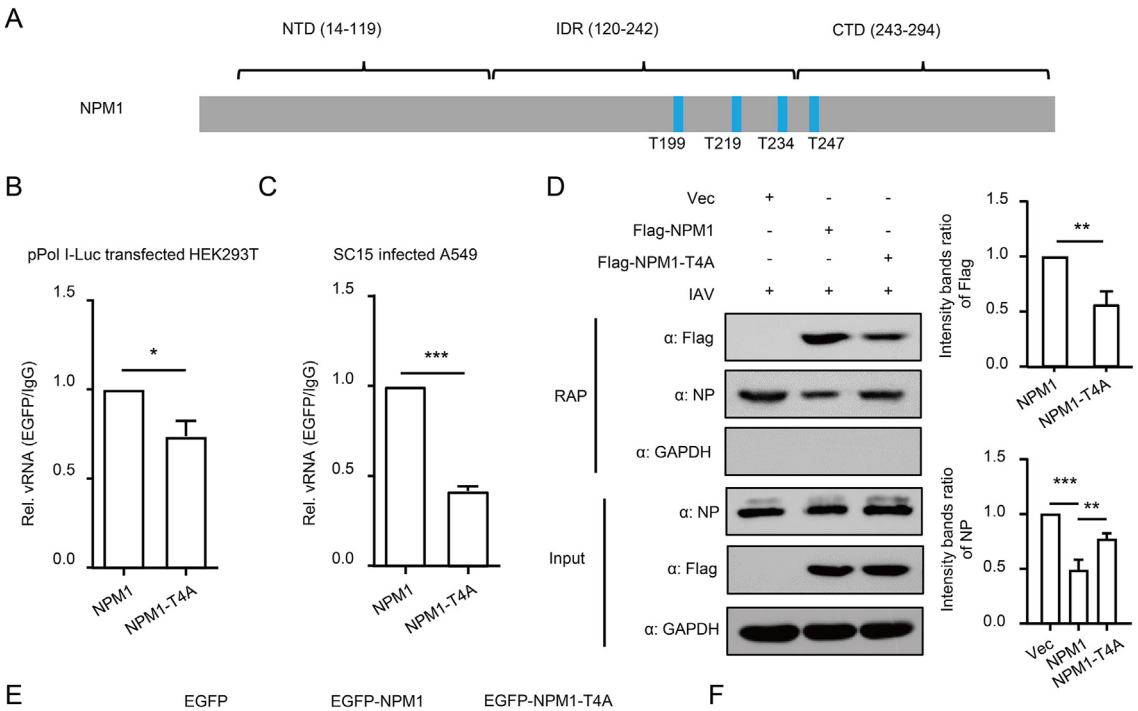

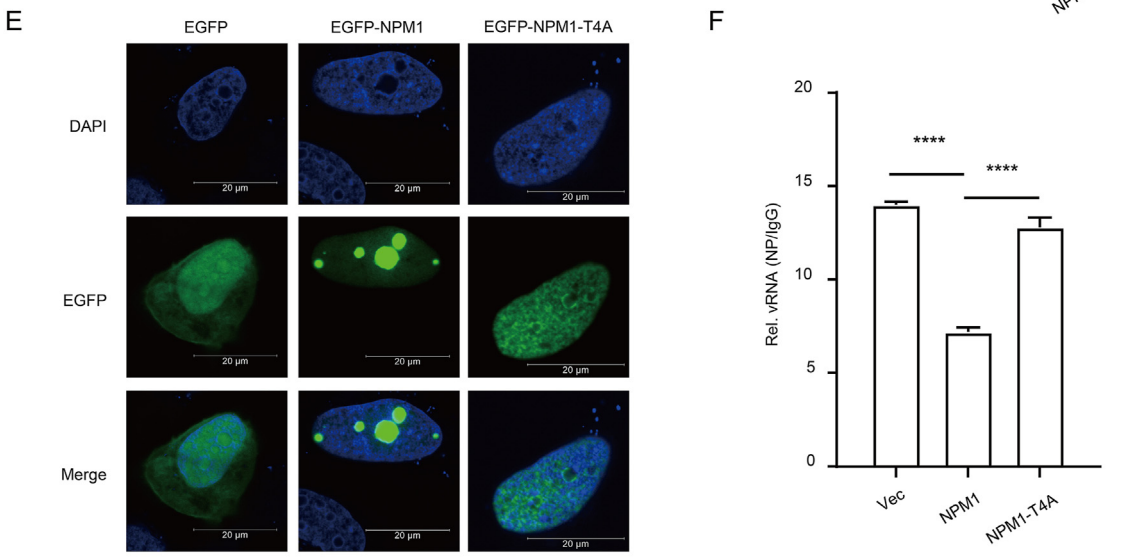

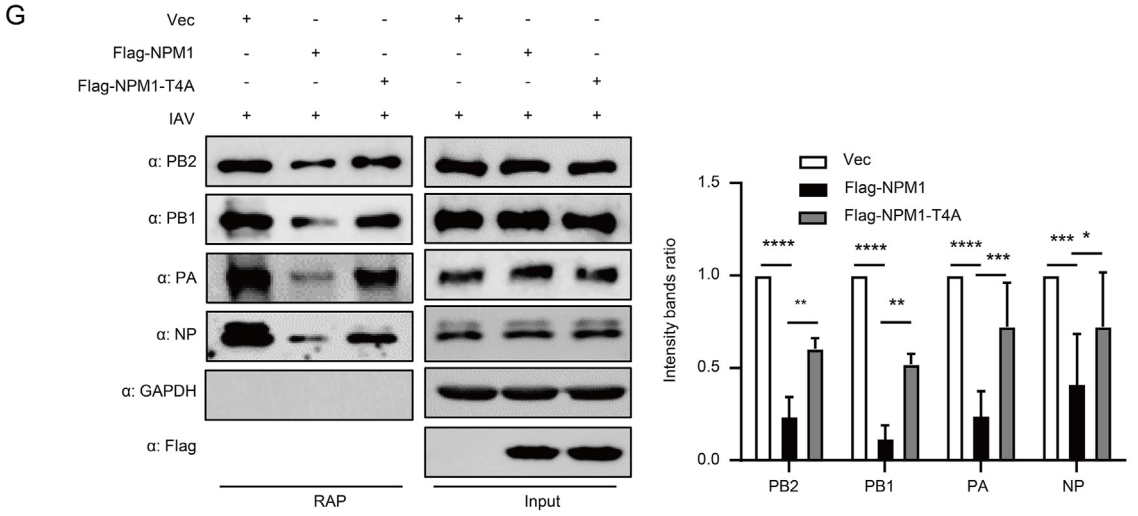

(caption on next page)

Fig. 5. The T4A mutant of NPM1 inhibits binding with viral RNAs. **A** The schematic representation shows NPM1 and NPM1-T4A, a mutant in which the threonine residues were replaced with alanine (A). **B** HEK293T cells were transfected with PB2, PB1, PA, NP, and pPolI-Luc constructs, together with either EGFP-NPM1 or EGFP-NPM1-T4A. Twenty-four hours later, the cells were subjected to a CLIP assay with EGFP-specific antibodies or IgG. The level of NP vRNA was quantified using a qPCR assay and normalized to IgG. **C** A549 cells were transfected with EGFP-NPM1 or EGFP-NPM1-T4A expression plasmids. The cells were then infected with SC15 strain at an MOI of 1. Twenty-four hours later, the cells were subjected to the CLIP assay with EGFP-specific antibodies or IgG. The level of NP vRNA was quantified using a qPCR assay, normalized to IgG. **D** HEK293T cells were transfected with NPM1 or NPM1-T4A expression plasmids. The cells were then infected with SC15 strain (MOI = 0.1 for Vec and NPM1-T4A, and MOI = 1 for Flag-NPM1) for 24 h and then crosslinked by glutaraldehyde solution. The biotin-labeled NP-vRNA probes were used to pull-down NP-vRNA binding proteins. The intensities of the Flag bands in RAP were determined using ImageJ. **E** U2OS cells were transfected with EGFP, EGFP-NPM1, or EGFP-NPM1-T4A. Twenty-four hours later, the cells were fixed with 4% paraformaldehyde and stained with DAPI before confocal microscopy. Scale bar: 20 μm. **F** HEK293T cells were transfected with PB2, PB1, PA, NP, and pPolI-Luc constructs, together with Vec, NPM1, or NPM1-T4A expression plasmids. Twenty-four hours later, the cells were subjected to a CLIP assay with NP-specific antibodies or IgG. **G** HEK293T cells were transfected with Vec, NPM1, or NPM1-T4A expression plasmids. Twenty-four hours later, cells were infected with SC15 strain (MOI = 0.1 for Vec and NPM1-T4A, and MOI = 1 for Flag-NPM1) for 24 h. Then, the cells were crosslinked by glutaraldehyde solution. Biotin-labeled NP-vRNA probes were used to pull-down NP-vRNA binding proteins. The intensities of the indicated bands in RAP were determined using ImageJ. The data shown represent three independent experiments; bars represent the mean ± SD of the three independent experiments (n = 3). *$P < 0.05$, **$P < 0.01$, ***$P < 0.001$, ****$P < 0.0001$; 'ns' indicates no significant difference.

CONCLUSIONS

In summary, we found that NPM1, a nucleolar-localized matrix protein, inhibits the replication of influenza A virus. In IAV-infected cells, NPM1 binds to vRNA and competes with vRNP proteins thereby suppressing polymerase activity and inhibiting IAV replication. This effect might be blocked by mutations that decrease the RNA-binding activity of NPM1. Overall, our findings highlight the role of NPM1 in IAV replication and identify NPM1 as a promising candidate for anti-influenza development strategies.

MATERIALS AND METHODS

Biosafety and ethical statements

Studies with H5N6 and H7N9 subtype avian influenza viruses were carried out in a biosecurity level 3 laboratory approved for such use by the Chinese Ministry of Agriculture and Rural Affairs. The protocol was approved by the Committee on the Ethics of Animal Experiments of the Harbin Veterinary Research Institute (HVRI) of the Chinese Academy of Agricultural Sciences (CAAS). The details of the facility and the biosafety and biosecurity measures used have been previously reported (Kong et al., 2021).

Cells, viruses, and plasmids

MDCK, HEK293T, U2OS, HeLa, and MRC5 cells purchased from American Type Culture Collection (ATCC) were grown in DMEM (Gibco) supplemented with 10% (vol/vol) FBS (Gibco-BRL; 10,099–141) and 1 × penicillin/streptomycin (Gibco-BRL; 10378016). A549 cells purchased from ATCC were grown in Kaighn's modified Ham F-12 nutrient mixture medium (Gibco) supplemented with 10% FBS and penicillin/streptomycin. All cells were cultured and maintained at 37 °C with 5% CO_2.

The H1N1 influenza A virus (A/Puerto Rico/8/1934, PR8) was stored in our laboratory. The H3N2 influenza virus (A/Swine/Shandong/TA05/2021) was kindly provided by Prof. Yihong Xiao (The Shandong Agricultural University, China). The H5N6 influenza A virus (A/Goose/Sichuan/SC15/2015, SC15) was isolated in Sichuan Province in China in 2015. The H7N9 virus (A/Suzhou/SZ19/2014, SZ19) was isolated from Jiangsu Province in China in 2014 (Zeng et al., 2021). The H9N2 virus (A/Chicken/Hunan/38/2018, HN38) was isolated from Hunan Province in China in 2018. Virus stocks were propagated in specific-pathogen-free (SPF) chicken eggs and stored at −70 °C until use.

Human NPM1 and NPM1 mutants (T199/219/234/237A) were constructed using standard molecular biology techniques. The genes encoding PB1, PB2, PA, and NP were amplified from the SC15 viral genome and then cloned into the pCAGGS vector. The plasmid pPolI-Luc, for the expression of a viral RNA-like firefly luciferase gene under the control of the human RNA polymerase I promoter, has been reported previously (Wang et al., 2025). The negative strands of viral NP genes were amplified and cloned into the plasmid pPol I, for the expression of vRNA under the control of the human RNA polymerase I promoter.

Reagents and antibodies

The antibodies used in this study were as follows: HRP-conjugated anti-HA (12013819001) antibody (Roche); rabbit anti-PB2 (GTX125926), anti-PB1 (GTX125923), and anti-PA (GTX118991) polyclonal antibodies (Genetex); anti-NP (11,675-MM03T) antibody (Sino Biological); HRP-conjugated goat anti-rabbit IgG (ZB-2301) (Proteintech); HRP-conjugated goat anti-mouse secondary antibody (ab102448), anti-NPM1 (ab52644) and anti-GAPDH (ab181602) antibodies (Abcam); HRP-conjugated anti-Flag (A8592) antibody (Sigma); and anti-GFP antibody (AF2882) (Beyotime).

Reagents used in the study included: anti-Flag agarose affinity beads (A2220) and protein A/G agarose affinity beads (P6486/E3403) (Sigma); and DAPI (C1002) and NP-40 (ST366) (Beyotime). The scrambled negative control RNA (NC) and NPM1-specific siRNA were purchased from RiboBio Co. (China). Lipofectamine 2000 and RNAi MAX were obtained from Invitrogen (USA). SYBR Green I Master Mix was purchased from Roche (Germany).

Viral infection

All cells were seeded at the desired density in culture plates as per the requirements for the different experiments. Viruses were inoculated into cells at the specified multiplicity of infection (MOI) for different experiments. One hour after inoculation, the medium was replaced with fresh OPTI-MEM, and the cells were incubated at 37 °C. Virus-containing culture supernatants were collected at the indicated timepoints for titration.

RNA isolation and qRT-PCR

Total RNA from cells or other samples was extracted using TRIzol, following the manufacturer's instructions. For cellular mRNAs, total RNA was subsequently transcribed into cDNA using M-MLV Reverse Transcriptase, according to the manufacturer's protocol (Promega). The levels of viral NP vRNA, cRNA, and mRNA were determined using a strand-specific real-time RT-PCR as described previously (Kawakami et al., 2011). GAPDH was used as a control for the normalization of cellular mRNA and intracellular viral RNA. Real-time PCR was carried out using the ABI 7500 Detection System (Applied Biosystems, USA). The RNA level of each gene is shown as the fold induction ($2^{-\Delta\Delta CT}$) in the graph. The sequences of primers used for qRT-PCR are shown in Supplementary Table S1.

Virus titration

Virus titers of virus stocks and cell culture supernatant were determined by end-point titration in MDCK cells or eggs. For end-point viral titration in

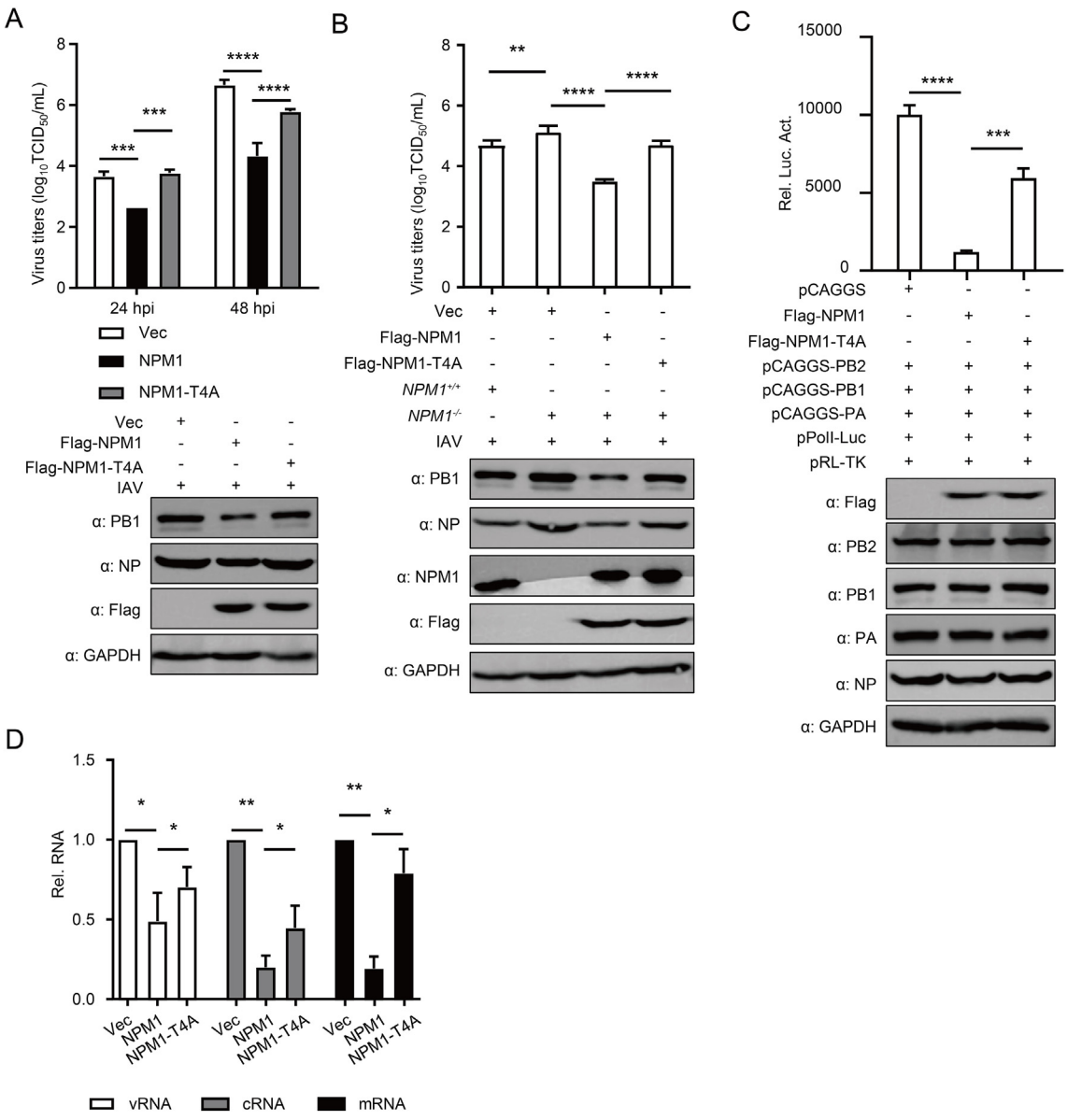

Fig. 6. The T4A mutant restored the inhibitory effect of NPM1 on the replication of influenza A virus. **A** A549 cells were transfected with Vec, NPM1, or NPM1-T4A. Twenty-four hours later, the cells were infected with SC15 strain at an MOI of 0.1. At the indicated times post-infection, the supernatant containing viral particles was assessed by using the TCID$_{50}$ assay. Expression levels of Flag-NPM1 and viral proteins were quantified. **B** *NPM1*$^{+/+}$ or *NPM1*$^{-/-}$ cells were transfected with Vec, NPM1, or NPM1-T4A. Twenty-four hours later, the cells were infected with SC15 strain at an MOI of 0.1. At 24 h post-infection, the supernatant containing viral particles was assessed using the TCID$_{50}$ assay. Expression levels of Flag-NPM1 and viral proteins were quantified. **C** Luciferase assay in HEK293T cells that were transfected with PB2, PB1, PA, NP, and pPolI-Luc and TK reporter constructs, together with Vec, NPM1, or NPM1-T4A expression plasmids. **D** A549 cells were transfected with Vec, NPM1, or NPM1-T4A. Twenty-four hours later, the cells were infected with SC15 strain (MOI = 1) for 24 h, and total RNA was extracted for qRT-PCR to detect the expression of NP vRNA, cRNA, or mRNA. The data shown represent three independent experiments; bars represent the mean ± SD of the three independent experiments (n = 3). *$P < 0.05$, **$P < 0.01$, ***$P < 0.001$, ****$P < 0.0001$; 'ns' indicates no significant difference.

MDCK cells, ten-fold serial dilutions of each sample were inoculated into MDCK cells. Two days after inoculation, supernatant from the inoculated cells was collected and tested for the ability to agglutinate chicken erythrocytes as an indicator of viral replication. Infectious virus titers are reported as log_{10} TCID$_{50}$/mL and were calculated from three replicates using the method of Reed-Muench (Matumoto, 1949). For end-point viral titration in eggs, 10-fold serial dilutions of each sample were inoculated into 9-day-old SPF eggs. Forty-eight hours after inoculation, fluid from the allantoic cavity was collected and tested for its ability to agglutinate chicken erythrocytes as an indicator of viral replication. Infectious virus titers are reported as log_{10} EID$_{50}$/mL and were calculated from three replicates using the method of Reed-Muench (Matumoto, 1949).

CRISPR-Cas9 knockout

Genome engineering was performed using the CRISPR-Cas9 system (Sanjana et al., 2014). Double-stranded oligonucleotides corresponding to the target sequences were cloned into the pX459 vector. Two micrograms of each pX459 plasmid containing one of the targeting sequences were simultaneously transfected into A549 cells. The transfected cells were selected with puromycin (1 μg/mL) for at least 7 days to obtain knockout cell pools. The following sequences were targeted for the human *NPM1* gene: 5′- AAAATTGCCATCTCTACCTGTGG -3′, 5′-AGGTGGTAGCAAGGTTCCACAGG -3′, and 5′-CAAGGTTCCACAGGTAGAGATGG -3′.

Dual-luciferase reporter assay

HEK293T cells were transfected with pCAGGS constructs expressing viral PB2, PB1, PA, and NP proteins, the construct pPolI-Luc, and an internal control pRL-TK (Promega), along with wild-type or mutant NPM1-expressing vectors. Cells were incubated at 37 °C for 24 h, and cell lysates were subsequently prepared using the Dual-Luciferase Reporter Assay System (Promega). The luciferase activities were measured on a GloMax 96 microplate luminometer (Promega) as reported previously (Li et al., 2021).

Cross-linking immunoprecipitation (CLIP)

At the indicated times post-infection or post-transfection, cells were cross-linked with 1% formaldehyde solution, and lysed in cell lysis buffer (10 mmol/L Tris-HCl pH 7.4, 10 mmol/L NaCl, 0.5% NP-40. 1 mmol/L DTT, 200 units/mL RNaseOUT, and EDTA-free Protease Inhibitor Cocktail). The cells were incubated in lysis buffer for 10 min on ice with frequent mixing and were sonicated to ensure maximum lysis. The lysed cell suspension was centrifuged for 5 min at 10,000 ×*g* at 4 °C. The supernatant was incubated with specific antibodies or IgG for 4 h at 4 °C. Then, the mixture was incubated with protein A/G magnetic beads and rotated for 4 h at 4 °C. After this incubation, the beads were washed three times with NT2 buffer (50 mmol/L Tris-HCl pH 7.4, 150 mmol/L NaCl, 1 mmol/L $MgCl_2$, 0.05% NP-40.), followed by incubation with 50 μg of proteinase K (Takara Bio) at 55 °C for 30 min. Input and co-immunoprecipitated RNAs were extracted by TRIzol, and analyzed by qPCR.

Fluorescence in situ hybridization (FISH)

The FISH probes corresponding to the vRNA of the *NP* gene were designed and synthesized with Cy3 label by Servicebio (Wuhan, China), and the FISH assay was performed using the SweAMI-fluorescence in situ hybridization kit (Servicebio) according to the manufacturer's protocol. Briefly, cells were seeded in 12-well plates on coverslips, and transfected or infected for 24 h before fixation. Cells were then washed three times with PBS, and incubated with pre-hybridization solution for 1 h. The pre-hybridization solution was then removed and replaced with probe-containing hybridization solution, and the cells were left overnight in the incubator. The cells were then washed with 2 × saline sodium citrate buffer (SSC), at 37 °C for 10 min, 1 × SSC, at 37 °C for 2 × 5 min, and 0.5 × SSC at room temperature for 10 min. Preheated corresponding branch probe hybridization solution was then added dropwise to the slides and incubated for 45 min at 40 °C. The cells were then washed again, and dropwise add the hybridization solution containing the signal probe. Then, the cells were stained with DAPI and observed with a Leica SP8 confocal microscopy (× 100 oil objective NA 1.40). The colocalization analysis was conducted with ImageJ software. The probe sequences are shown in Table S1.

RNA antisense purification (RAP) assay

For the RAP assay, a RAP Kit (BersinBio, Guangzhou, China) was used by following the manufacturer's protocol. The probes corresponding to the vRNA of the *NP* gene were synthesized with biotin tags located at the 5′ end by RiboBio (RiboBio Biotechnology). Briefly, cross-linked cells were lysed, sonicated, and then hybridized with the probe for 4 h at 37 °C. The hybridization mixture was then treated with magnetic beads. After that, the bound proteins were cleaned and analyzed by Western blotting.

Western blotting

Cells or protein samples were lysed in RIPA buffer (Beyotime, China). Proteins were separated by 10% SDS-PAGE and transferred to a nitrocellulose membrane (Bio-Rad). The membrane was blocked for 1 h in TBST containing 5% milk and subsequently incubated with primary Abs overnight at 4 °C. After a 1-h incubation with HRP-conjugated secondary antibody, the immunoreactive bands were visualized using an ECL system (GE Healthcare). The intensities of the target bands were quantified using the Image J program (NIH, USA).

Co-immunoprecipitation

HEK293T cells were co-transfected with the indicated plasmids with or without virus infection for 24 h. The transfected cells were then harvested and lysed in NP-40 lysis buffer [20 mmol/L Tris-HCl (pH 7.5), 150 mmol/L NaCl, 1% NP-40, 1 mmol/L EDTA with protease inhibitor cocktails]. For each immunoprecipitation, 1 mL of lysate or lysate mixture was incubated for 4 h at 4 °C with 0.5 μg of the indicated antibody or control IgG and 30 μL of protein A/G-Sepharose (Sigma). The beads were washed three times with 1 mL of lysis buffer containing 500 mmol/L NaCl. The precipitates were analyzed using standard immunoblotting procedures.

In vitro polymerase activity assay

The *in vitro* viral polymerase activity assay was conducted as reported previously (Wang et al., 2025). Briefly, viral particle was purified as mentioned above, and lysed in a lysis buffer [50 mmol/L Tris-HCl, (pH 7.5), 150 mmol/L NaCl, 5 mmol/L $MgCl_2$, 0.5% NP-40, 1 mmol/L DTT, 200 units/mL RNaseOUT, and EDTA-free Protease Inhibitor Cocktail] to prepare virion vRNP (vvRNP). At the indicated time points post-transfection of NPM1 plasmid, cells were washed by PBS for three times, and lysed in lysis buffer. Equal volume of vvRNP and cell lysate were normally incubated at 30 °C overnight (for maximum sensitivity) in the presence of 1 mmol/L ATP, 0.5 mmol/L of each CTP, GTP, and UTP, 5 mmol/L $MgCl_2$, 1 mmol/L DTT, and 200 units/mL RNaseOUT. RNA was extracted with TRIzol reagent and subsequently reverse-transcribed into cDNA with Oligo dT or viral strand-specific RT primers. The expression of viral positive-strand RNA was normalized with actin.

Statistical analyses

Data are expressed as the mean ± standard deviation (SD). Statistical significance was determined using the Student's two-tailed unpaired *t-test* or an analysis of variance (ANOVA) with GraphPad Prism software (version 6.0, San Diego, CA, USA). Differences between groups were considered significant when the *P* value was <0.05 (*), <0.01 (**), <0.001 (***), and <0.0001 (****).

DATA AVAILABILITY

All the data generated during the current study are included in this paper.

ETHICS STATEMENT

This article does not contain any studies with human or animal subjects performed by any of the authors.

AUTHOR CONTRIBUTIONS

Yingying Yu: data curation, formal analysis, investigation, and validation. Qian Wang: data curation, formal analysis, investigation, and validation. Yanli Wei: data curation, investigation, and methodology. Junwen Liu: data curation, investigation, and validation. Guangwen Wang: investigation and resources. Zhengxiang Wang: data curation and investigation. Wentao Shen: data curation and investigation. Lu Han: data curation and investigation. Chengjun Li: methodology and resources. Cao-Qi Lei: methodology and resources. Shuai Xu:

conceptualization, funding acquisition, methodology, project administration, supervision, writing-original draft, writing-review & editing. Qiyun Zhu: conceptualization, funding acquisition, project administration, resources, supervision, writing-review & editing.

CONFLICT OF INTEREST

The authors declare that they have no conflict of interest.

ACKNOWLEDGMENTS

We thank Susan Watson for editing the manuscript. We appreciate the gift of the H3N2 virus from Prof. Yihong Xiao at the Shandong Agricultural University (China). This study was supported by funding from the National Natural Science Foundation of China (U23A20243 and 32272972 to QZ, 32172820 to SX), the Major Science and Technology Project of Gansu Province (22ZD6NA001 to SX), the Youth Innovation Program (Y2023QC30) and the Agricultural Science and Technology Innovation Program (CAAS-ASTIP-JBGS-20210102 to SX) of the Chinese Academy of Agricultural Sciences.

APPENDIX A. SUPPLEMENTARY DATA

Supplementary data to this article can be found online at https://doi.org/10.1016/j.virs.2025.04.007.

REFERENCES

Borer, R.A., Lehner, C.F., Eppenberger, H.M., Nigg, E.A., 1989. Major nucleolar proteins shuttle between nucleus and cytoplasm. Cell 56, 379–390.
Bortz, E., Westera, L., Maamary, J., Steel, J., Albrecht, R.A., Manicassamy, B., Chase, G., Martinez-Sobrido, L., Schwemmle, M., Garcia-Sastre, A., 2011. Host- and strain-specific regulation of influenza virus polymerase activity by interacting cellular proteins. mBio 2, e00151-11.
Chiarella, S., De Cola, A., Scaglione, G.L., Carletti, E., Graziano, V., Barcaroli, D., Lo Sterzo, C., Di Matteo, A., Di Ilio, C., Falini, B., Arcovito, A., De Laurenzi, V., Federici, L., 2013. Nucleophosmin mutations alter its nucleolar localization by impairing G-quadruplex binding at ribosomal DNA. Nucleic Acids Res. 41, 3228–3239.
Chiem, K., Rangel-Moreno, J., Nogales, A., Martinez-Sobrido, L., 2019. A luciferase-fluorescent reporter influenza virus for live imaging and quantification of viral infection. J. Vis. Exp. https://doi.org/10.3791/59890.
De Rozieres, C.M., Pequeno, A., Shahabi, S., Lucas, T.M., Godula, K., Ghosh, G., Joseph, S., 2022. PABP1 drives the selective translation of influenza A virus mRNA. J. Mol. Biol. 434, 167460.
Eisfeld, A.J., Neumann, G., Kawaoka, Y., 2015. At the centre: influenza A virus ribonucleoproteins. Nat. Rev. Microbiol. 13, 28–41.
Fan, H., Walker, A.P., Carrique, L., Keown, J.R., Serna Martin, I., Karia, D., Sharps, J., Hengrung, N., Pardon, E., Steyaert, J., Grimes, J.M., Fodor, E., 2019. Structures of influenza A virus RNA polymerase offer insight into viral genome replication. Nature 573, 287–290.
Gadad, S.S., Rajan, R.E., Senapati, P., Chatterjee, S., Shandilya, J., Dash, P.K., Ranga, U., Kundu, T.K., 2011. HIV-1 infection induces acetylation of NPM1 that facilitates Tat localization and enhances viral transactivation. J. Mol. Biol. 410, 997–1007.
Gao, R., Cao, B., Hu, Y., Feng, Z., Wang, D., Hu, W., Chen, J., Jie, Z., Qiu, H., Xu, K., Xu, X., Lu, H., Zhu, W., Gao, Z., Xiang, N., Shen, Y., He, Z., Gu, Y., Zhang, Z., Yang, Y., Zhao, X., Zhou, L., Li, X., Zou, S., Zhang, Y., Li, X., Yang, L., Guo, J., Dong, J., Li, Q., Dong, L., Zhu, Y., Bai, T., Wang, S., Hao, P., Yang, W., Zhang, Y., Han, J., Yu, H., Li, D., Gao, G.F., Wu, G., Wang, Y., Yuan, Z., Shu, Y., 2013. Human infection with a novel avian-origin influenza A (H7N9) virus. N. Engl. J. Med. 368, 1888–1897.
Hisaoka, M., Nagata, K., Okuwaki, M., 2014. Intrinsically disordered regions of nucleophosmin/B23 regulate its RNA binding activity through their inter- and intramolecular association. Nucleic Acids Res. 42, 1180–1195.
Karimi Dermani, F., Gholamzadeh Khoei, S., Afshar, S., Amini, R., 2021. The potential role of nucleophosmin (NPM1) in the development of cancer. J. Cell. Physiol. 236, 7832–7852.
Kato, H., Takeuchi, O., Sato, S., Yoneyama, M., Yamamoto, M., Matsui, K., Uematsu, S., Jung, A., Kawai, T., Ishii, K.J., Yamaguchi, O., Otsu, K., Tsujimura, T., Koh, C.S., Reis E Sousa, C., Matsuura, Y., Fujita, T., Akira, S., 2006. Differential roles of MDA5 and RIG-I helicases in the recognition of RNA viruses. Nature 441, 101–105.
Kawakami, E., Watanabe, T., Fujii, K., Goto, H., Watanabe, S., Noda, T., Kawaoka, Y., 2011. Strand-specific real-time RT-PCR for distinguishing influenza vRNA, cRNA, and mRNA. J. Virol. Methods 173, 1–6.
Kong, X., Guan, L., Shi, J., Kong, H., Zhang, Y., Zeng, X., Tian, G., Liu, L., Li, C., Kawaoka, Y., Deng, G., Chen, H., 2021. A single-amino-acid mutation at position 225 in hemagglutinin attenuates H5N6 influenza virus in mice. Emerg. Microb. Infect. 10, 2052–2061.
Krammer, F., Schultz-Cherry, S., 2023. We need to keep an eye on avian influenza. Nat. Rev. Immunol. 23, 267–268.
Lakdawala, S.S., Wu, Y., Wawrzusin, P., Kabat, J., Broadbent, A.J., Lamirande, E.W., Fodor, E., Altan-Bonnet, N., Shroff, H., Subbarao, K., 2014. Influenza a virus assembly intermediates fuse in the cytoplasm. PLoS Pathog. 10, e1003971.
Li, J., Liang, L., Jiang, L., Wang, Q., Wen, X., Zhao, Y., Cui, P., Zhang, Y., Wang, G., Li, Q., Deng, G., Shi, J., Tian, G., Zeng, X., Jiang, Y., Liu, L., Chen, H., Li, C., 2021. Viral RNA-binding ability conferred by SUMOylation at PB1 K612 of influenza A virus is essential for viral pathogenesis and transmission. PLoS Pathog. 17, e1009336.
Matumoto, M., 1949. A note on some points of calculation method of LD50 by Reed and Muench. Jpn. J. Exp. Med. 20, 175–179.
Mayer, D., Molawi, K., Martinez-Sobrido, L., Ghanem, A., Thomas, S., Baginsky, S., Grossmann, J., Garcia-Sastre, A., Schwemmle, M., 2007. Identification of cellular interaction partners of the influenza virus ribonucleoprotein complex and polymerase complex using proteomic-based approaches. J. Proteome Res. 6, 672–682.
Melen, K., Tynell, J., Fagerlund, R., Roussel, P., Hernandez-Verdun, D., Julkunen, I., 2012. Influenza A H3N2 subtype virus NS1 protein targets into the nucleus and binds primarily via its C-terminal NLS2/NoLS to nucleolin and fibrillarin. Virol. J. 9, 167.
Nguyen, N.L.T., Wu, W., Pante, N., 2023. Contribution of the nuclear localization sequences of influenza A nucleoprotein to the nuclear import of the influenza genome in infected cells. Viruses 15, 1641.
Okuwaki, M., Tsujimoto, M., Nagata, K., 2002. The RNA binding activity of a ribosome biogenesis factor, nucleophosmin/B23, is modulated by phosphorylation with a cell cycle-dependent kinase and by association with its subtype. Mol. Biol. Cell 13, 2016–2030.
Pederson, T., 2011. The nucleolus. Cold Spring Harbor Perspect. Biol. 3.
Pradeep, P., Sivakumar, K.C., Sreekumar, E., 2023. Host factor nucleophosmin 1 (NPM1/B23) exerts antiviral effects against chikungunya virus by its interaction with viral nonstructural protein 3. Microbiol. Spectr. 11, e0537122.
Prinos, P., Lacoste, M.C., Wong, J., Bonneau, A.M., Georges, E., 2011. Mutation of cysteine 21 inhibits nucleophosmin/B23 oligomerization and chaperone activity. Int J Biochem Mol Biol 2, 24–30.
Sakashita, G., Kiyoi, H., Naoe, T., Urano, T., 2018. Analysis of the oligomeric states of nucleophosmin using size exclusion chromatography. Sci. Rep. 8, 4008.
Saluri, M., Leppert, A., Gese, G.V., Sahin, C., Lama, D., Kaldmae, M., Chen, G., Elofsson, A., Allison, T.M., Arsenian-Henriksson, M., Johansson, J., Lane, D.P., Hallberg, B.M., Landreh, M., 2023. A "grappling hook" interaction connects self-assembly and chaperone activity of Nucleophosmin 1. PNAS Nexus 2, pgac303.
Sanjana, N.E., Shalem, O., Zhang, F., 2014. Improved vectors and genome-wide libraries for CRISPR screening. Nat. Methods 11, 783–784.
Stauber, R.H., Pavlakis, G.N., 1998. Intracellular trafficking and interactions of the HIV-1 Tat protein. Virology 252, 126–136.
Sun, H., Li, H., Tong, Q., Han, Q., Liu, J., Yu, H., Song, H., Qi, J., Li, J., Yang, J., Lan, R., Deng, G., Chang, H., Qu, Y., Pu, J., Sun, Y., Lan, Y., Wang, D., Shi, Y., Liu, W.J., Chang, K.C., Gao, G.F., Liu, J., 2023. Airborne transmission of human-isolated avian H3N8 influenza virus between ferrets. Cell 186, 4074–4084 e11.
Suspene, R., Petit, V., Puyraimond-Zemmour, D., Aynaud, M.M., Henry, M., Guetard, D., Rusniok, C., Wain-Hobson, S., Vartanian, J.P., 2011. Double-stranded RNA adenosine deaminase ADAR-1-induced hypermutated genomes among inactivated seasonal influenza and live attenuated measles virus vaccines. J. Virol. 85, 2458–2462.
Taubenberger, J.K., Kash, J.C., 2010. Influenza virus evolution, host adaptation, and pandemic formation. Cell Host Microbe 7, 440–451.
Terrier, O., Carron, C., De Chassey, B., Dubois, J., Traversier, A., Julien, T., Cartet, G., Proust, A., Hacot, S., Ressnikoff, D., Lotteau, V., Lina, B., Diaz, J.J., Moules, V., Rosa-Calatrava, M., 2016. Nucleolin interacts with influenza A nucleoprotein and contributes to viral ribonucleoprotein complexes nuclear trafficking and efficient influenza viral replication. Sci. Rep. 6, 29006.
Wang, H., Shi, D., Jiang, P., Yu, Z., Han, Y., Zhang, Z., Wang, P., Huang, H., Yao, H., Qian, P., 2022. SARS-CoV-2 N protein potentiates host NPM1-snoRNA translation machinery to enhance viral replication. Signal Transduct. Targeted Ther. 7, 356.
Wang, Q., Xu, S., Shen, W., Wei, Y., Han, L., Wang, Z., Yu, Y., Liu, M., Liu, J., Deng, G., Chen, H., Zhu, Q., 2025. N6-methyladnosine of vRNA facilitates influenza A virus replication by promoting the interaction of vRNA with polymerase proteins. Proc. Natl. Acad. Sci. U. S. A. 122, e2411554122.
Wasik, B.R., Voorhees, I.E.H., Parrish, C.R., 2021. Canine and feline influenza. Cold Spring Harb. Perspect. Med. 11, a038562.
Yan, Y., Du, Y., Wang, G., Li, K., 2017. Non-structural protein 1 of H3N2 influenza A virus induces nucleolar stress via interaction with nucleolin. Sci. Rep. 7, 17761.
Yang, J., Yan, J., Zhang, C., Li, S., Yuan, M., Zhang, C., Shen, C., Yang, Y., Fu, L., Xu, G., Shi, W., Ma, Z., Luo, T.R., Bi, Y., 2023. Genetic, biological and epidemiological study on a cluster of H9N2 avian influenza virus infections among chickens, a pet cat, and humans at a backyard farm in Guangxi, China. Emerg. Microb. Infect. 12, 2143282.
Zeng, Y., Xu, S., Wei, Y., Zhang, X., Wang, Q., Jia, Y., Wang, W., Han, L., Chen, Z., Wang, Z., Zhang, B., Chen, H., Lei, C.Q., Zhu, Q., 2021. The PB1 protein of influenza A virus inhibits the innate immune response by targeting MAVS for NBR1-mediated selective autophagic degradation. PLoS Pathog. 17, e1009300.
Zhang, T., Yin, C., Boyd, D.F., Quarato, G., Ingram, J.P., Shubina, M., Ragan, K.B., Ishizuka, T., Crawford, J.C., Tummers, B., Rodriguez, D.A., Xue, J., Peri, S., Kaiser, W.J., Lopez, C.B., Xu, Y., Upton, J.W., Thomas, P.G., Green, D.R., Balachandran, S., 2020. Influenza virus Z-RNAs induce ZBP1-mediated necroptosis. Cell 180, 1115–1129 e13.
Zhang, Y., Zhang, Q., Kong, H., Jiang, Y., Gao, Y., Deng, G., Shi, J., Tian, G., Liu, L., Liu, J., Guan, Y., Bu, Z., Chen, H., 2013. H5N1 hybrid viruses bearing 2009/H1N1 virus genes transmit in Guinea pigs by respiratory droplet. Science 340, 1459–1463.

Zhou, J., Dai, Y., Lin, C., Zhang, Y., Feng, Z., Dong, W., Jin, Y., Yan, Y., Zhou, J., Gu, J., 2020. Nucleolar protein NPM1 is essential for circovirus replication by binding to viral capsid. Virulence 11, 1379–1393.
Zhou, J., Li, J., Li, H., Zhang, Y., Dong, W., Jin, Y., Yan, Y., Gu, J., Zhou, J., 2021. The serine-48 residue of nucleolar phosphoprotein nucleophosmin-1 plays critical role in subcellular localization and interaction with porcine circovirus type 3 capsid protein. Vet. Res. 52, 4.
Zhu, Y., Wang, R., Zou, J., Tian, S., Yu, L., Zhou, Y., Ran, Y., Jin, M., Chen, H., Zhou, H., 2023. N6-methyladenosine reader protein YTHDC1 regulates influenza A virus NS segment splicing and replication. PLoS Pathog. 19, e1011305.